Gyrokinetic Particle Simulation

of

Ion Temperature Gradient Drift Instabilities

W. W. Lee and W. M. Tang

Plasma Physics Laboratory, Princeton University

Princeton, New Jersey 08544

ABSTRACT

Ion temperature gradient drift instabilities have been investigated using gyrokinetic particle simulation techniques for the purpose of identifying the mechanisms responsible for their nonlinear saturation as well as the associated anomalous transport. For simplicity, the simulation has been carried out in a shear-free slab geometry, where the background pressure gradient is held fixed in time to represent quasistatic profiles typical of tokamak discharges. It is found that the nonlinearly generated zero-frequency responses for the ion parallel momentum and pressure are the dominant mechanisms giving rise to saturation. This is supported by the excellent agreement between the simulation results and those obtained from mode coupling calculations, which give the saturation amplitude as $\left| e\phi/T_e \right| \cong (\left| \omega_\ell + i\gamma_\ell \right|/\Omega_i)/(k_\perp \rho_s)^2$, and the quasilinear thermal diffusivity as $\chi_i \cong \gamma_\ell/k_\perp^2$, where ω_ℓ and γ_ℓ are the linear frequency and growth rate, respectively, for the most unstable mode of the system. In the simulation, the time evolution of χ_i after saturation is characterized by its slow relaxation to a much lower level of thermal conduction. On the other hand, a small amount of electron-ion collisions, which has negligible effect on the linear stability, can cause significant enhancement of χ_i in the steady state.

MASTER

I. INTRODUCTION

As emphasized in the early review by Kadomtsev and Pogutse,[1] anomalous ion thermal losses associated with ion temperature gradient drift instabilities,[2,3] have long been regarded as a potentially serious threat to efficient magnetic confinement. These are basically electrostatic waves associated with the ion acoustic branch which can become destabilized when the parameter, $\eta_i =$ $d(\ln T_i)/d(\ln n_i)$, exceeds a critical value (usually estimated to be between 1 and 2). Recent results from a variety of important tokamak experiments[4-6] have stimulated renewed interest in establishing the relevance of η_i-modes as the primary cause of the observed anomalous ion conduction. The evidence generally indicates that when plasma conditions are consistent with larger values of η_i, the corresponding deterioration in the ion thermal confinement properties cannot be explained by standard neoclassical transport theory. On the other hand, anomalous transport models based on very simple estimates of the thermal diffusivity (χ_i) for η_i-modes have produced results in reasonable agreement with these experimental trends.[7-10] Since the level of confidence in the predictive capability of any transport model is dependent on its "first principles" (as opposed to heuristic or empirical) physics content, it is obviously of vital importance to understand properly the processes responsible for the nonlinear saturation of the η_i-modes and for the associated steady-state transport. To this end, a gyrokinetic particle code[11] has been developed to investigate the dynamic properties of these instabilities.

As just noted, experimental data from tokamaks are at least consistent with the possible degradation of thermal confinement associated with η_i-driven instabilities. In particular, the saturation of the energy confinement time, τ_E, with increasing density in ohmically heated discharges can be explained by invoking

DISCLAIMER

standard ion neoclassical transport for situations when the η_i-parameter is not too large.[12,13] However, if (as in cases of high density plasmas fuelled by gas puffing [4,5]) the density profiles become sufficiently flat, the resultant enhancement of η_i correlates with the "anomalous" saturation of τ_E at densities well below those predicted by the neoclassical calculations. Furthermore, in cases of high density pellet-fuelled plasmas, the observed improvement of τ_E (over the gas-fuelled cases just described) correlates well with the fact that the steepened density profiles lead to smaller values of η_i.[14] With regard to plasmas heated by neutral beam injection (NBI), data analysis again indicates that the ion thermal losses generally exceed standard neoclassical estimates.[15] Moreover, recent experimental studies[6] involving direct measurement of the ion temperature profile in the D-III tokamak have indicated that the thermal diffusivity is not only much larger in magnitude but also exhibits a radial dependence in strong disagreement with the usual neoclassical model (χ_i^{NEO}).

The idea that the well-known η_i-type instabilities could be responsible for the thermal confinement trends observed in pellet-fuelled and gas-fuelled ohmic discharges was first proposed by Coppi.[7] Using the simplest nonlinear models for χ_i associated with toroidal η_i-modes, Dominguez and Waltz[8] and Romanelli et al.[9] have demonstrated in transport code studies that the saturation of τ_E with increasing density could indeed be correlated with the presence (or absence) of these instabilities in numerous ohmically heated tokamaks. When invoked in NBI-heated discharges, η_i-modes also lead to scalings of temperatures and confinement times in reasonable agreement with experimental trends.[10]

With regard to the formal theoretical basis in support of the relevance of the η_i-modes, linear studies generally indicate that they should be present under

3

typical operating conditions in tokamaks, provided η_i is sufficiently large. Although the exact value of the η_i-threshold is very difficult to calculate,[16] numerical results from comprehensive fully toroidal linear calculations (including complete trapped-particle dynamics, wave-particle resonant interactions, and collisions) support the conclusion that these modes are easily destabilized in tokamaks for $\eta_i \gtrsim 2$.[17]

An appropriate expression for the anomalous thermal diffusivity associated with η_i-modes is, of course, much more difficult to justify from "first principles." At the simplest level, heuristic strong-turbulence-based arguments[1] can be made to obtain the familiar estimate for the thermal diffusivity, $\chi_i \propto \gamma_\ell/k_\perp^2$, with γ_ℓ being the linear growth rate of the strongest mode in the unstable spectrum and $k_\perp$ being the corresponding perpendicular wave number. More formally, but in the same spirit as this estimate, the anomalous thermal flux can be calculated[18] using the linearized perturbed distribution function together with the usual ambient gradient or mixing length approximation for the saturated amplitude of the perturbations. An expression quite similar to the $\gamma_\ell/k_\perp^2$ answer generally results and is the most common form applied in various transport studies.[7-10,19] Although they lead to plausible models for the anomalous ion diffusivity, these calculations leave open fundamental physics questions regarding the identification of the specific mechanisms responsible for the saturation process and for the enhanced steady-state transport.

In developing a detailed theory of η_i-driven turbulent transport, the simplest approach is to consider the fluid limit where the dynamics are governed by a Boltzmann response for the electrons and by the hydrodynamic (fluid) equations for density, parallel velocity, and pressure of the ions. This approach is motivated by

4

the fact that when η_i lies well above the linear threshold $[\eta_i > (\eta_i)_c \sim 1$ to 2], it is commonly believed[20-23] that the fluid model reasonably approximates the relevant dynamics. However, kinetic effects (such as those associated with ion Landau damping) are likely to play a prominent role for conditions approaching marginal stability. The nonlinear fluid-type analysis as applied to η_i-modes was introduced in the work of Horton et al.,[20] who carried out three-dimensional initial value simulations for a sheared slab configuration. Their results indicated that profile flattening associated with nonlinear $E \times B$ convection of the ion pressure was primarily responsible for saturation. This is similar to the profile-modified saturated states commonly observed in conventional particle code simulations of these instabilities.[24] However, this is not a realistic scenario since the equilibrium ("steady state") profiles in actual confined plasmas are in fact maintained by continuous heating and refuelling effects. Fixed-profile 3D fluid simulation studies of η_i-modes are currently in progress.[25]

With regard to nonlinear analytic calculations, Horton et al.[21] have carried out a mode-coupling analysis of η_i-modes for a simplified system of nonlinear fluid equations applied to a toroidal geometry. Solutions for the saturated amplitudes are in basic agreement with the heuristic mixing length results described earlier. In more recent work, Lee and Diamond[22] have analyzed a nonlinear system of fluid equations applied to a sheared slab geometry and have produced a renormalized theory describing saturated η_i-driven turbulence. Although the final results are again similar to the mixing-length estimate, the authors emphasize the necessity of including the ion viscous term (ignored in Refs. 20, 21, and 23) to consistently ensure a finite-amplitude steady-state solution. In particular, they note that the saturated stationary turbulence results from the energy transfer process which nonlinearly couples the long-wavelength energy source with the short-wavelength energy sink (which is proportional to the parallel viscosity). Finally, following a very different line of analysis, Connor[23] has

5

pointed out that the invariance properties of the fluid equations (studied in Refs. 20 and 22), regardless of the details of the nonlinear calculations, can be used to determine the transport scaling of η_i-driven turbulence for a sheared slab system. As in all the other papers discussed,[19-22] the local anomalous diffusivity is found to scale basically as $\chi_i \propto T^{3/2}/B^2 L$, with L being a characteristic equilibrium scale length. However, the specific magnitude of χ_i and the particular prescription for L are different in the various evaluations.

As indicated by the preceding discussion, considerable progress has been made in recent years, and these efforts will undoubtedly contribute to the eventual development of a reliable "predictive" model for anomalous transport. In the present paper, η_i-driven instabilities have been investigated using newly developed gyrokinetic particle simulation techniques.[11] Unlike previous attempts on the problem,[19-23,25] the present approach does not require prior assumptions concerning the nature of the instability (kinetic vs. fluid), nor does it need any prejudgment as to the relative importance of the nonlinear effects involved. As such, it affords us the opportunity to identify the relevant nonlinear mechanisms on a totally unbiased basis. As described in Ref. 11, the new technique is far more superior numerically in terms of time step, grid spacing, and noise level than the conventional particle codes for simulating low frequency microinstabilities. Most importantly, by employing the scheme of multiple spatial scale expansion, it becomes possible to use a "frozen" background inhomogeneity in the simulation. Thus, one can study the truly steady-state problems without the undesirable effect of quasilinear profile modification. For simplicity, we have chosen to carry out the simulation in slab geometry without shear. This is an adequate approximation, since, without toroidal-coupling effects, the usual sheared slab model with single helicity as used in Ref. 24 tends to overestimate the effect of shear stabilization for $\eta_i \gg 1$.[16] Moreover, from an analytical point of view, the inclusion of shear will unduly complicate the nonlinear physics issues.

The paper is organized as follows. In Sec. II the governing equations and the linear properties for η_i-modes are presented. Simulation results from an electrostatic two-dimensional gyrokinetic particle code are given in Sec. III. The theoretical interpretation of the simulation results based on the mode coupling calculations of the governing equations and their conservation properties is described in Sec. IV. A summary of the main findings in these studies together with the concluding remarks are given in Sec. V.

II. GOVERNING EQUATIONS AND LINEAR PROPERTIES

Nonlinear gyrokinetic equations for the Vlasov-Poisson system in slab geometry have been used earlier for studying drift instabilities in the presence of a density gradient.[26] The same set of equations is utilized here as the starting point for the investigation of η_i-modes. In the usual gyrokinetic units of ρ_s, Ω_i^{-1}, and T_e/e for length, time, and potential, the governing equations in the limit of $(k_\perp \rho_i)^2 \ll 1$ can be written as[11,26]

$$Df_e/Dt + L_e F_{Me} = C(f_e), \tag{1}$$

$$Df_i/Dt + (1 + \nabla_\perp^2/\tau) L_i F_{Mi} + (\nabla_\perp^2/\tau) \nabla \Phi \times \hat{b} \cdot \hat{x} \kappa_{Ti} F_{Mi} = 0. \tag{2}$$

$$\nabla_\perp^2 \Phi + n_i = n_e. \tag{3}$$

where $f_\alpha(x, v_\parallel, t)$ is the perturbed distribution, α denotes species, $F_{M\alpha} = (1/\sqrt{2\pi} v_{t\alpha}) \exp[-(v_\parallel/v_{t\alpha})^2]$, $\hat{b} = B/B$, B is the ambient magnetic field, $\hat{x}$ is the unit vector in the inhomogeneous direction perpendicular to B, $\tau = T_e/T_i$, $\nabla = \partial/\partial x$.

7

and

$$n_\alpha = \int f_\alpha dv_{\parallel} \qquad (4)$$

is the perturbed number density. The perpendicular Laplacian acting on Φ accounts for the finite Larmor radius effects for the ions and it supersedes the usual Debye shielding term in Eq. (3). For Eqs. (1) and (2), we also have

$$Df_\alpha/Dt = \partial f_\alpha/\partial t + v_{\parallel}\hat{\mathbf{b}}\cdot\nabla f_\alpha - \nabla\Phi\times\hat{\mathbf{b}}\cdot\nabla f_\alpha - s_\alpha\nabla\Phi\cdot\hat{\mathbf{b}}\partial f_\alpha/\partial v_{\parallel}. \qquad (5)$$

$$L_\alpha F_{M\alpha} = -s_\alpha\nabla\Phi\cdot\hat{\mathbf{b}}\,\partial F_{M\alpha}/\partial v_{\parallel} + \nabla\Phi\times\hat{\mathbf{b}}\cdot\hat{\mathbf{x}}[\kappa_n - \kappa_{T\alpha}/2 + (v_{\parallel}/v_{t\alpha})^2\kappa_{T\alpha}/2]F_{M\alpha}. \qquad (6)$$

$$C(f_e) = \nu_{ei}(\partial/\partial v_{\parallel})(v_{te}^2\partial f_e/\partial v_{\parallel} + v_{\parallel}f_e), \qquad (7)$$

where $s_e = -m_i/m_e$, $s_i = 1$, $\kappa_n = -d\ln n_0/dx$, and $\kappa_{T\alpha} = -d\ln T_{0\alpha}/dx$ are the zeroth-order spatial inhomogeneities, which give $\eta_\alpha = \kappa_{T\alpha}/\kappa_n$, and ν_{ei} is the electron-ion collision frequency. [Note that, in our units, $v_{te} = \sqrt{m_i/m_e}$ and $v_{ti} = 1/\sqrt{\tau}$.] Equation (7), which can easily be obtained from the Lorentz collision operator by assuming that $v_{\perp}$ remains Maxwellian for the perturbed distribution, is the usual number-density-conserving one-dimensional diffusion model.[26] Equations (1)-(7) are a simplified set of gyrokinetic equations, which includes both E×B and velocity space nonlinearities essential for describing steady-state microturbulence. Linearly, the resulting dispersion relation for η_i-modes includes the critical wave-particle resonances and, thus, predicts the correct threshold for the onset of the instability [cf., Ref. 24].

For certain instances, simplified fluid responses are adequate for describing the instability, such as collisional drift waves and ion temperature gradient modes

for $\eta_i \gg 1$. The governing equations in those cases can be obtained by taking velocity moments of Eqs. (1) and (2). Using the definitions

$$\int v_{\parallel} f_{\alpha} dv_{\parallel} \simeq u_{\alpha}, \tag{8}$$

$$\int (v_{\parallel} - u_{\alpha})^2 f_{\alpha} dv_{\parallel} = v_{t\alpha}^2 p_{\alpha}. \tag{9}$$

and neglecting higher order nonlinearities and velocity moments, we arrive at

$$dn_e/dt + \partial u_e/\partial x_{\parallel} + (\partial \phi/\partial y)\kappa_n = 0, \tag{10}$$

$$du_e/dt + (m_i/m_e)\partial(p_e - \Phi)/\partial x_{\parallel} = -\nu_{ei} u_e, \tag{11}$$

and

$$dp_e/dt + \partial u_e/\partial x_{\parallel} + (\partial \phi/\partial y)(\kappa_n + \kappa_{Te}) = 0. \tag{12}$$

These are, respectively, the continuity, momentum, and pressure balance equations for the electrons, where

$$d/dt = \partial/\partial t - \nabla \Phi \times \hat{b} \cdot \nabla, \tag{13}$$

and the E×B convection term is the only nonlinearity retained in the formulation. The corresponding equations for the ions can be written as

$$dn_i/dt + \partial u_i/\partial x_{\parallel} + (\partial \phi/\partial y)[\kappa_n + (\nabla_{\perp}^2/\tau)(\kappa_n + \kappa_{Ti})] = 0, \tag{14}$$

$$du_i/dt + (1/\tau)\partial p_i/\partial x_{\parallel} + (1 + \nabla_{\perp}^2/\tau)\partial \phi/\partial x_{\parallel} = 0, \tag{15}$$

and

$$dp_i/dt + \partial u_i/\partial x_{\parallel} + (\partial \phi/\partial y)[(\kappa_n + \kappa_{Ti}) + (\nabla_{\perp}^2/\tau)(\kappa_n + 2\kappa_{Ti})] = 0, \tag{16}$$

9

which differ slightly from the electron fluid equations because of the finite
Larmor radius effects. Equations (10)-(16) together with Eq. (3) can adequately
describe a wide range of microturbulence problems. For example, for $\kappa_{T\alpha} = 0$, they
can be reduced to the well-known equations studied by Hasegawa and Mima,[27] and
Hasegawa and Wakatani.[28] Compared with the equations used by Horton et al.,[20] Lee
and Diamond,[22] and Connor.[23] the major difference is in the nonlinear E×B term in
the continuity equation. Eqs. (10) and (14), where n_α has been replaced by p_α.

These two sets of equations (kinetic and fluid) are the basis for the
investigation of η_i-modes. Since we are mainly interested in the cases of $\eta_i \gg$
1, for which $v_{ti} \ll |\omega/k_\parallel| \ll v_{te}$, the linear dispersion relation, based on the
fluid ions and adiabatic electrons ($n_e = \tilde{\phi}$), and with the ansatz of exp(ik·x-iωt),
becomes

$$1 + \tau b - [1-b(1+\eta_i)]\omega_*/\omega$$
$$- (k_\parallel v_{ti}/\omega)^2[\tau(1-b)+(1+\eta_i)\omega_*/\omega-b(1+2\eta_i)\omega_*/\omega] = 0, \qquad (17)$$

where $b = (k_\perp \rho_i)^2$ accounts for the gyroradius effects, $k_\perp^2 = k_x^2 + k_y^2$, and $\omega_* =$
$k_y \rho_s \kappa_n \rho_s \Omega_i$ is the electron diamagnetic drift frequency. Equation (17) can also be
obtained directly from Eqs. (2) and (3) by taking the fluid limit for the ion
parallel motion [see, for example, Ref. 24]. By letting $b = -\rho_i^2 \partial^2/\partial x^2 + (k_y \rho_i)^2$ and
$k_\parallel = k_y x/L_s$, where L_s is the shear scale length, one then recovers the linear
eigenmode equation used by Connor (although, with some minor differences).[23] For
$b = 0$ and $\omega_* = 0$, i.e., $\eta_i = \infty$, Eq. (17) reduces to[1]

$$(\tau + \omega_{*Ti}/\omega)(k_\parallel v_{ti}/\omega)^2 = 1, \qquad (18)$$

where $\omega_{*Ti} = k_y \rho_s \kappa_{Ti} \rho_s \Omega_i$. For $|\omega_{*Ti}/\omega| \gg \tau$, there exists an unstable mode with

$$\omega/\omega_{*Ti} \approx (\omega_\ell + i\gamma_\ell)/\omega_{*Ti} = (k_\parallel v_{ti}/\omega_{*Ti})^{2/3}(-1 + i\sqrt{3})/2. \qquad (19)$$

Since the real frequency is negative, the mode propagates in the ion diamagnetic direction. For $\omega_{*Ti} = 0$, Eq. (18) predicts stable ion acoustic oscillations.

When the electron temperature gradient is also present, i.e., $\eta_e \neq 0$, the linear electron density response given by Eq. (1) takes the form of

$$n_e(k) = \phi(k)[1 - i\sqrt{\pi/2}(\omega_* - \omega_{*Te}/2 - \omega_\ell)/k_\parallel v_{te}], \qquad (20)$$

where $\omega_{*Te} = k_y \rho_s \kappa_{Te} \rho_s \Omega_i$. Since $|\omega/k_\parallel v_{te}| \ll 1$, the correction to the dispersion relations, Eqs. (17) and (18), due to the nonadiabatic part of the response is negligible. The effect of weak collisions, $|\nu_{ei}/k_\parallel v_{te}| \ll 1$, on the linear stability of η_i-modes is also small, which can be easily verified by following the procedures described in Ref. 26 for solving Eqs. (1) and (7) in the Fourier-transformed velocity space. Nevertheless, both finite η_e and collisions are believed to have some influence on particle and energy transport.

When the collisions are strong, i.e., $|\nu_{ei}/k_\parallel v_{te}| \gg 1$ and $|\omega\nu_{ei}/(k_\parallel v_{te})^2| \ll 1$, the electron response can be described by Eqs. (10)-(12). For $\kappa_n = \kappa_{Te} = 0$, we have

$$n_e(k) = \phi(k)[1 + i\omega_\ell \nu_{ei}/(k_\parallel v_{te})^2]. \qquad (21)$$

11

Again, the net influence on Eqs. (17) and (18) is insignificant. Although this limit of collisionality is beyond the regime of interest for our simulation, we will later take advantage of the simplicity of these equations in formulating steady-state transport properties for η_i-modes. Since Eqs. (10)-(16) are not energy conserving, they are not suitable for describing the effects of an electron temperature gradients on the η_i-instabilities.

Under the present gyrokinetic formulation, the quantities related to plasma transport are rather easy to evaluate. From Eqs. (8)-(16), with the Klimontovich representation for f_α, we obtain the particle and thermal fluxes as[11]

$$\langle \Gamma_{\alpha x} \rangle = \langle n_\alpha v_{Ex} \rangle = \text{Im} \sum_k k_y [n_\alpha(k)]^* \phi(k) = \sum_{j=1}^N v_{Ex}(x_j)/N \tag{22}$$

and

$$\langle Q_{\alpha x} \rangle = \langle p_\alpha v_{Ex} \rangle = \text{Im} \sum_k k_y [p_\alpha(k)]^* \phi(k) \equiv \sum_{j=1}^N (v_{\|j}/v_{t\alpha})^2 v_{Ex}(x_j)/N, \tag{23}$$

respectively, where $v_{Ex} = -\partial\phi/\partial y$ is the E×B drift in the x direction, $\langle \ \rangle = \int dx/V$ denotes spatial average, x_j is the position of the j-th particle, and N is the total number of particles in the simulation. Upon invoking the scheme of multiple spatial scale expansion,[11,29] one can then express the corresponding particle diffusion coefficient and the thermal diffusivity as

$$D_\alpha = \langle \Gamma_{\alpha x} \rangle / \kappa_n \tag{24}$$

and

$$\chi_\alpha = \langle Q_{\alpha x} \rangle / (\kappa_{T\alpha} + \kappa_n). \tag{25}$$

The material presented in this section forms the basis for our investigation of η_i-modes in Secs. III and IV.

III. GYROKINETIC PARTICLE SIMULATION

Simulation techniques for gyrokinetic plasmas have been reported in detail in Ref. 11. Briefly, both the electrons and the ions are treated as guiding center particles. The only difference between the two species comes from the fact that the ions are advanced in time with a gyrophase-averaged potential, whereas the electrons are under the influence of a bare potential. Density responses due to ion polarization effects are then accounted for in the field (Poisson) equation. The instability is driven by an external source in the form of a time-independent background inhomogeneity, so as to eliminate the undesirable effect of profile modification in the nonlinear stage of the development. To simulate the Lorentzian collision processes, the scheme of pitch-angle scattering for the guiding-center electrons is used.[26] In the regime of $(k_\perp \rho_i)^2 \ll 1$, the behavior of the simulation plasma can essentially be described by Eqs. (1)-(3).

In this paper, we will present the results from a two-dimensional gyrokinetic electrostatic code $[x, y, v_\parallel, \mu (=v_\perp^2/2)]$ in a shearless slab. For simplicity, periodic boundary conditions for both the waves and the particles are assumed. The ambient magnetic field is given by $\mathbf{B} = B_0(\hat{\mathbf{b}} + \theta \hat{\mathbf{y}})$ with θ being a small constant ($\ll 1$), which gives $k_\parallel = \theta k_y$, and the plasma inhomogeneity is in the x direction. In the code we have also set $\Phi(k_x \neq 0, k_y = 0) = 0$ and $\Phi(k_x = 0, k_y \neq 0) = 0$. The latter is necessitated by the requirement of $|\kappa_n|$ or $|\kappa_{T\alpha}| < |k_x|$ for a system with a "frozen" zeroth-order gradient.[11]

When the adiabatic electron response is assumed, we can totally ignore the electron dynamics by letting

$$\delta n_e(x)/n_0 = [1 + \langle \delta n_e(x)/n_0 \rangle_y]e\Phi(x)/T_e + \langle \delta n_e(x)/n_0 \rangle_y. \tag{26}$$

13

in the field equation, where $\langle \ \rangle_y$ denotes a spatial average in y, and δn_α and n_0 are the perturbed and the averaged number densities, respectively. The condition of $\Phi(k_x \neq 0, k_y = 0) = 0$ makes Eq. (26) number conserving and also calls for the use of the high electron mobility model,[24] which assumes that

$$\langle \delta n_e(x) \rangle_y = \langle \delta \overline{n}_i(x) \rangle_y, \tag{27}$$

where $\delta \overline{n}_i$ is the gyrophase-averaged ion number density[11] and $\delta \overline{n}_i \cong \delta n_i$ for $(k_\perp \rho_i)^2 \ll 1$. [Note that $\delta n_\alpha/n_0 \rightarrow n_\alpha$ and $e\Phi/T_e \rightarrow \Phi$ in Sec. II.]

The simulation parameters in units of grid size Δ and ion cyclotron frequency Ω_i are: $L_x \times L_y = 16\Delta \times 16\Delta$, N(total number of simulation particles per species) = 128×128, $\rho_s/\Delta = 1$, a(particle size)$/\Delta = 1.5$, $T_e/T_i = 1$, $m_i/m_e = 1837$, $(k_x \rho_s, k_y \rho_s)$ = $(0.393m, 0.393n)$, $(m,n) = 0, \pm 1, \pm 2, ...$, $\theta \equiv k_\parallel/k_y = 0.01$, $\kappa_{Ti}\rho_s = 0.2$, $\kappa_{Te}\rho_s = 0$ or 0.2, $\kappa_n \rho_s = 0$ or 0.05, (i.e., $\omega_{*Ti}/\Omega_i = 0.08n$, $\omega_{*Te}/\Omega_i = 0$ or $0.08n$, $\omega_*/\Omega_i = 0$ or $0.02n$), and $\Omega_i \Delta t$(time step) = 2.722. The total number of time steps ranges from $t_{max}/\Delta t = 1000$ to 4000.

The time step and the number of particles used for the simulation are determined from numerical stability and noise considerations. This requires that $\omega_H \Delta t \tilde{<} 1$ and $|e\Phi/T_e|_{t=0} = 1/\sqrt{N} k\rho_s \ll |e\Phi/T_e|_{t=\infty} \cong \rho_s/L_T$,[11] where $\omega_H/\Omega_i = (k_\parallel/k)(m_i/m_e)^{1/2}$ is the electrostatic version of the shear-Alfvén wave and N is the total number of particles in one wavelength of the mode. Thus, for the (m=1,n=1) mode, we have $\omega_H \Delta t = 0.82$ and $|e\Phi/T_e| = 1.38\%$, which are well within these numerical limits. It should be pointed out here that the time step and grid size

used here are equivalent to $\omega_{pe}\Delta t = 5,000$ and $\lambda_{De}/\Delta = 1/42.86$ for $\Omega_e/\omega_{pe} = 1$. In the case of an adiabatic response for the electrons, we can afford to use an even longer time step with less simulation particles, i.e., $\Omega_i \Delta t = 10.89$ and $N = 64 \times 64$. This is because the restrictions imposed by ω_H are now replaced by those from the ion acoustic modes (or η_i-modes).

Let us first examine the case for $\eta_i = \infty$ and $\eta_e = 0$ ($\kappa_{Ti}\rho_s = 0.2$, $\kappa_{Te} = \kappa_n = 0$), using the adiabatic electron model of Eqs. (26) and (27). The complex linear frequencies for the $(m=1,n=\pm1)$ modes given by Eq. (19) are

$$(\pm\omega_\ell + i\gamma_\ell)/\Omega_i = -0.0054 + i0.0094. \tag{28}$$

Since $\left|\omega_\ell/k_\parallel v_{ti}\right| = 1.35$, the fluid approximation used here for the ions is not totally adequate. A more elaborate calculation based on the kinetic description for the parallel ion motion[24] indeed gives slightly different answers. More importantly, the calculation has shown that these modes are the fastest growing ones in the simulation with the rest being either weakly unstable or damped modes. This linear prediction agrees with the simulation results as indicated by the fluctuating k-spectrum for the potential, in which the most unstable modes of the system indeed dominate. The reason is that the fastest growing modes in our system also have the longest wavelengths and, as such, inverse energy cascade is prohibited. The time history ($\Omega_i t = 0-2,700$) and the frequency spectra for $\Phi(m=1,n=\pm1)$ are shown in Fig. 1. These are rather coherent oscillations which follow roughly the prescribed linear properties of the η_i-instability. Although the two modes do not exponentiate and saturate at the same time, they do reach the same saturation amplitude of $\left|e\Phi/T_e\right| \tilde{=} 5\%$, accompanied by a slight increase in amplitude to 6% and a frequency shift to $\omega/\Omega_i \tilde{=} \pm0.012$ after saturation. The

corresponding density fluctuations are $\delta n_i(1,1)/n_0 \tilde{=} \delta n_i(1,-1)/n_0 \tilde{=}$ 10-12%. In

addition, density perturbations of $\delta n_i(2,0)/n_0 \tilde{=}$ 10% with $\omega \tilde{=} 0$ and $\delta n_i(0,2)/n_0 \tilde{=}$

10% with $\omega/\Omega_i \tilde{=} \pm 0.024$ have also been observed in the steady state after

saturation. One unique feature shown in Fig. 1 is the process of energy exchange

between the two dominant modes in the nonlinear stage of the development. These

nonlinear properties of the instability will be examined in detail in Sec. IV.

To verify the results based on the adiabatic electrons (Fig. 1), we have also

carried out the simulation with the drift kinetic treatment of electrons for $\eta_i =$

$\eta_e = \infty$ ($\kappa_{Ti}\rho_s = \kappa_{Te}\rho_s = 0.2$, $\kappa_n = 0$). The time evolution for the dominant

potentials is shown in Fig. 2, where a bandpass filter with the width of ω_{*Ti} has

been used to eliminate the high frequency noise generated by the ω_H modes. As we

can see, the two results are nearly identical for both the linear and nonlinear

stages of development.. (The slight phase difference is caused by the difference in

the initial noise level.) The amplitude for the accompanied ion density fluctuations

also remains the same. The dominant electron density responses after saturation

assume the level of $\delta n_e(1,1)/n_0 = \delta n_e(1,-1)/n_0 \tilde{=}$ 5-7% and $\delta n_e(2,0)/n_0 \tilde{=}$ 4%.

Interestingly, unlike its ion counterpart, $\delta n_e(0,2)/n_0$ stays around the thermal level

of 1.4% throughout the simulation. These results also confirm the prediction of Eq.

(20) that $\eta_e \neq 0$ has a negligible effect on the linear stability of the mode.

However, its presence can give rise to inward particle transport for the electrons

as indicated by Eqs. (20) and (22).[19] The results shown in Fig. 2 clearly illustrate

this property in the linear stage of the instability. However, the flux reverses its

direction after saturation for the apparent reason that the electron behavior ceases

to be linear at this point in time. Since particle flux is ambipolar in the

simulation, i.e., $\langle\Gamma_{ex}\rangle = \langle\Gamma_{ix}\rangle$,[11] the ions have the same behavior. The calculation

for the particle flux in the code was based on Eq. (22).

The message from the simulation thus far is that one can probably describe the saturation of the instability with the adiabatic electron model, since all the necessary nonlinearities are provided by the ions. However, is such a model adequate for representing steady-state phenomena? To answer this question, we now study the long-time behavior of the instability ($\Omega_i t$ = 0-22,000) again with the adiabatic electrons for $\eta_i = \eta_e = 4$ ($\kappa_{Ti}\rho_s = \kappa_{Te}\rho_s = 0.2$, $\kappa_n\rho_s = 0.05$). The results indicate that the general feature of the instability is very similar to the cases shown in Figs. 1 and 2. The fluctuation spectra are also dominated by the same modes. Figure 3 gives the time history of the potential $\Phi(1,-1)$ and the resulting ion thermal flux. [The flux calculation in the code used the total v in Eq. (23) instead of $v_\parallel$. Consult Eq. (41) in Ref. 11 for details.] The linear frequency and the growth rate are nearly identical to the previous results and reflect the fact that the linear properties are rather insensitive to the magnitude of η_i when $\eta_i \gg 1$. The nonlinear frequency shift also remains the same. The amplitude for $e\Phi/T_e$ increases from about 5% at saturation to 9% at the end of the run. This may indicate that the system has yet to evolve to a steady state because of the simplified electron dynamics. The most interesting aspect of the results is the time plot for the ion thermal flux $\langle Q_{ix} \rangle$ in Fig. 3, for which a bandpass filter has been applied to eliminate the shot noise. The salient features are: 1) the time-averaged flux is always in the outward direction; 2) $\langle Q_{ix} \rangle/c_s$ reaches its maximum value of 0.0032 (0.0043 before filtering) around the time of saturation; 3) a precipitous (ten-fold) drop in its magnitude follows shortly after saturation; and 4) the thermal flux eventually attains a steady-state value which corresponds to $\chi_i \cong 8\times10^{-4} cT_e/eB$ as given by Eq. (25). The results here bring into question the validity of using the quasilinear flux to predict the steady-state transport.

17

We now proceed to examine the same case ($\eta_i = \eta_e = 4$) but with the drift kinetic treatment for the electrons. The comparison of the two results should help us gain a better understanding of the nonlinear behavior of the electrons. The length of the run is shorter than before with $\Omega_i t = 0$–11,000. Again, the overall characteristics of the instability during the linear as well as the nonlinear phase of the evolution are very similar to the previous run. Figure 4 exhibits the time history of the potential for the $(1,\pm1)$ modes, in which the thermal (numerical) noise caused by the high frequency (ω_H) oscillations are evident. [Note that $\left|e\Phi/T_e\right| \tilde{=} 1.2\%$ at t=0 as predicted.] Here, the time-averaged fluctuation amplitude after saturation is about 5% and the nonlinear frequencies are around $\omega/\Omega_i \tilde{=} \pm0.01$. The slight drop in amplitude toward the end of the run is believed to be the result of the slow amplitude modulation, which will become more evident later. The thermal flux vs. time plots for both species are given in Fig. 5, in which a filter with the width of ω_{Ti} has been applied to smooth the data for the electrons but not for the ions. These results indicate: 1) the electron thermal flux reaches its steady-state value shortly after saturation and the corresponding thermal diffusivity is $\chi_e \tilde{=} 1.2\times10^{-4}\ cT_e/eB$; 2) the relaxation of the quasilinear ion flux after saturation is much more gradual than the previous run; 3) however, the magnitude of the steady-state thermal diffusivity remains unchanged, i.e., $\chi_i \tilde{=} 8\times10^{-4}\ cT_e/eB$. In addition, the time-averaged particle flux is found to be outward and $D \tilde{=} 10^{-4}\ cT_e/eB$ is the magnitude of the diffusion coefficient in the steady-state. (Note that $D = 0$ for the case with the adiabatic electrons.) Since χ_i is the same for the two cases and $\chi_i \gg \chi_e \tilde{=} D$, one can reasonably conclude that the nonadiabatic response of the electrons is not essential for η_i-modes. Unfortunately (from the theoretical point of view), this is true only when the plasma is collisionless.

To ascertain the collisional effects on η_i-modes, we have carried out the same simulation ($\eta_i = \eta_e = 4$) with $\nu_{ei}/\Omega_i = 0.005$. Since $\omega \overset{>}{\sim} \nu_{ei}$ and $\nu_{ei}/k_\parallel v_{te}$ << 1, this is a weakly collisional case and the linear properties of the mode under investigation are not expected to change. [As indicated by Eq. (21), even strong collisions have negligible effects on the linear stability.] Thus, our focus here is on the nonlinear stage of development. The time evolution of $\Phi(1,\pm 1)$ for the collisional case is shown in Fig. 6. Although the amplitude at saturation increases slightly, the mean amplitude in the steady state stays around 5%, which is the same as the collisionless value. The major differences between the two runs are the energy exchange processes of the two dominant modes and the amplitude modulation of the total potential, $\left|\Phi(1,1)\right|^2 + \left|\Phi(1,-1)\right|^2$, both of which are significantly enhanced by the collisions. Consequently, the resulting oscillations in the nonlinear stage become less coherent with $\left|\Delta\omega/\omega\right| \sim 1$, $\omega(1,1)/\Omega_i \overset{\sim}{=} -0.01$ and $\omega(1,-1)/\Omega_i \overset{\sim}{=} -0.0075$. The net result is an increase in thermal transport for both the electrons and the ions as shown in Fig. 7. A closer examination of the results reveals that 1) the electron thermal flux, for which a filter has been applied, follows the amplitude modulation of the potential with $\chi_e \overset{\sim}{=} 4.8 \times 10^{-4} cT_e/eB$ as the mean value in the steady state; 2) the ion thermal flux also follows the amplitude modulation, and the steady-state thermal diffusivity is $\chi_i \overset{\sim}{=} 6.4 \times 10^{-3} cT_e/eB$; and 3) the time history for the particle flux (not shown) closely resembles that of the electron thermal flux with $D \overset{\sim}{=} 2.4 \times 10^{-3} cT_e/eB$ for $t = \infty$. All in all, there is a 4 to 24-fold increase in plasma transport, in which ion thermal conduction still dominates, i.e., $\chi_i > D >> \chi_e$ (although D exhibits the largest increase). Hence, in steady state situations the electron-ion collisions are here found to significantly enhance the transport associated with η_i-modes. This feature, which emphasizes the indispensible role played by the nonadiabatic electrons, has usually been ignored in previous nonlinear studies of these instabilities.

19

IV. THEORETICAL ANALYSIS OF SATURATION AND TRANSPORT

In this section, we intend to provide some theoretical understanding of the nonlinear behavior of the η_i-modes observed in the simulation. The main areas of investigation are: 1) the identification of the mechanisms responsible for the saturation; 2) the scaling of the resulting quasilinear transport; 3) the nature of steady-state transport as prescribed by the conservation properties of the governing equations; and 4) the transport scaling based on the invariance properties of the these equations.

We will first consider the issue of saturation. Since the potential fluctuation spectrum in the simulation is dominated by only a small number of Fourier k-modes, i.e., $\Phi(1,\pm1) + $ c. c., and since using the adiabatic approximation for the electrons leads to correct results for the saturated amplitudes, a set of simplified equations can be used in this analysis. It can be shown that the primary nonlinear consequence arising from the excitation of $\Phi(1,\pm1)$ is the generation of $f_i(\pm2,0)$ through the E×B convection. Moreover, the E×B convection together with the velocity space nonlinearity for the ions gives rise to the enhancement of $f_i(0,\pm2)$. If one assumes that $\Phi(1,1) = \Phi^*(1,-1)$, $f_i(1,1) = [f_i(1,-1)]^*$, and ignores the velocity space nonlinearity, $f_i(0,2)$ vanishes, and the reduced equations describe a three-mode coupling process. (Interested readers should consult Refs. 26 and 29 for details.) These approximations not only make the problem analytically tractable but also yield useful results.

Letting $n_e = \Phi$, $\omega_* = \omega_{*Te} = 0$, and $(k_\perp \rho_s)^2 \ll 1$, and denoting $(1,1)$ and $(2,0)$ by the subscripts of $+$ and 0, respectively, we can write Eqs. (2) and (3) as

$$\partial f_{i+}/\partial t + ik_\parallel v_\parallel f_{j+} + i[\tau k_\parallel v_\parallel - \omega_{*T}/2 + (v_\parallel/v_{ti})^2 \omega_{*T}/2]F_{Mi}\Phi_+ + k_\perp^2 \Phi_+ f_{i0} = 0. (29)$$

$$\partial f_{i0}/\partial t = 2i k_\perp^2 \text{Im}(\phi_+^* f_{i+}), \qquad (30)$$

$$n_{i+} = \phi_+, \qquad (31)$$

where $\phi_0 = 0$ is assumed, $n_{i+} = \int f_{i+} dv_\parallel$ is the ion density, $k_\perp^2 \equiv \tau b = 2k_x k_y$, and k_x, k_y are the wave numbers for the $(1,1)$ mode. Equations (29)-(31) can be solved by treating the nonlinear $E \times B$ terms as perturbations. With $\partial/\partial t = -i\omega$ and $|k_\parallel v_\parallel/\omega| \ll 1$, a nonlinear dispersion relation can then be obtained. A simpler and more transparent procedure is to use the equivalent fluid equations from Eqs. (14)-(16), i.e..

$$\partial n_{i+}/\partial t + i k_\parallel u_{i+} = 0, \qquad (32)$$

$$\partial u_{i+}/\partial t + i k_\parallel \phi_+ + i k_\parallel p_{i+}/\tau + k_\perp^2 \phi_+ u_{i0} = 0, \qquad (33)$$

$$\partial u_{i0}/\partial t = 2i k_\perp^2 \text{Im}(\phi_+^* u_{i+}) \qquad (34)$$

$$\partial p_{i+}/\partial t + i k_\parallel u_{i+} + i\omega_{*Ti}\phi_+ + k_\perp^2 \phi_+ p_{i0} = 0, \qquad (35)$$

$$\partial p_{i0}/\partial t = 2i k_\perp^2 \text{Im}(\phi_+^* p_{i+}). \qquad (36)$$

Equation (32) is linear, because $n_{i+} = \phi_+$, which gives $\partial n_{i0}/\partial t = 0$. For $\partial/\partial t = -i\omega$ and $|k_\parallel v_{ti}/\omega| \ll 1$, we obtain

$$p_{i+} \tilde{=} (\omega_{*Ti}/\omega)\phi_+, \qquad (37)$$

which, together with the linear responses from Eqs. (31)-(33), gives us the linear

21

dispersion relation of Eq. (18). The nonlinearly excited parallel fluid velocity and pressure are proportional to the amplitude of the potential and can be expressed as

$$u_{i0} = i(k_{\perp}' |\phi_+|)^2 / k_{\parallel} \tag{38}$$

and

$$p_{i0} = 2i\omega_{\ell}(k_{\perp} |\phi_+|)^2/(k_{\parallel}v_{t i})^2 = -i(k_{\perp}|\phi_+|)^2 \omega_{*Ti}/|\omega_{\ell}+i\gamma_{\ell}|^2, \tag{39}$$

where $\omega_{\ell}+i\gamma_{\ell}$ is the linear (complex) frequency given by Eq. (19). The nonlinear dispersion relation for η_i- modes can then be written as

$$(\tau + \omega_{*Ti}/\omega)(k_{\parallel}v_{t i}/\omega)^2 + (1+2\omega_{\ell}/\omega) k_{\perp}^4 |\phi_+|^2/\omega^2 = 1. \tag{40}$$

which remains a cubic equation in ω. An alternative form for Eq. (40) can be obtained by using the second expression for p_{i0} in Eq. (39). To satisfy the stability requirement, $\text{Im}\,\omega = 0$, Eq. (40) yields that

$$|\phi_+| = (\sqrt{3}/2)|\omega_{\ell}+i\gamma_{\ell}| / k_{\perp}^2 = (\sqrt{3}/2)[(k_{\parallel}v_{t i})^2 \omega_{*Ti}]^{1/3}/ k_{\perp}^2. \tag{41}$$

This is the appropriate saturation amplitude of the instability. The nonlinear frequency now becomes

$$\omega_{n\ell}/\omega_{*Ti} = -2|\omega_{\ell}+i\gamma_{\ell}|/\omega_{*Ti} = -2(k_{\parallel}v_{t i}/\omega_{*Ti})^{2/3}. \tag{42}$$

which yields an upward frequency shift. Equation (40) can also be derived from Eqs. (29)-(31) by keeping the first two nonvanishing terms from the expansion of the resonant denominator; the other terms in the expansion are negligible. We now compare these theoretical predictions with the simulation results shown in Fig. 1. Substituting Eq. (28) in Eqs. (41) and (42), we find that $|\phi_+| = 3\%$ and $\omega_{n\ell}/\Omega_i = $

22

0.022, whereas the measured values are 5% and 0.012, respectively. The cause for the small discrepancy is the absence of the ion kinetic (velocity space) effects in the mode-coupling equations, which would nonlinearly generate $\tilde{r}_i(0,\pm2)$ and, in turn, render $\Phi(1,1) \neq \Phi^*(1,-1)$.[26,29] Nonetheless, the calculation presented here veritably captures the primary features of the saturation process in the simulation.

The quasilinear particle and thermal transport can be calculated as follows. Substituting Eq. (20) into Eq. (22), we have

$$\langle \Gamma_{ex} \rangle = \sqrt{\pi/2} \sum_{\mathbf{k}} k_y |\Phi(\mathbf{k})|^2 (\omega_* - \omega_\varrho - \omega_{*Te}/2)/k_\parallel v_{te} \tag{43}$$

for the quasilinear particle flux due to the η_i-instability. For $\eta_e > 2(1-\omega_\varrho/\omega_*)$, the flux is negative and the particle transport is directed inward.[19] Based on the results from Eq. (28) for ω_ϱ and Eq. (41) for $|\Phi(\mathbf{k})|$, we obtain $\langle \Gamma_{ex} \rangle/c_s = -3.5 \times 10^{-4}$ as the particle flux due to $\Phi_\pm$ and their complex conjugates at saturation for $\eta_i = \eta_e = \infty$. This is much greater than the results shown in Fig. 2, indicating that the nonadiabatic response of the electrons deviates considerably from Eq. (20) even in the linear stage of the instability. Equation (43) is also not applicable to the results associated with those given in Figs. 4-7 for $\eta_i = \eta_e = 4$, where the particle flux is outwardly directed even before saturation, with or without collisions. (Note that quasilinear estimates would indicate that collisions should actually enhance inward transport.)

The ion thermal diffusivity, which can be obtained by substituting Eq. (37) into Eqs. (23) and (25), takes the form

$$\chi_i = \sum_{\mathbf{k}} |k_y |\Phi(\mathbf{k})|^2 \gamma_\varrho / |\omega_\varrho + i\gamma_\varrho|^2. \tag{44}$$

23

This expression is also valid for $\kappa_n \neq 0$. From Eq. (41), which gives the saturation level for $\Phi_{\pm}$ and their complex conjugates, the quasilinear coefficient then becomes

$$\chi_i = (3/2) \, \gamma_\ell / k_\perp^2. \tag{45}$$

Using the linear growth rate from Eq. (28), we have $\chi_i = 0.044 \, cT_e/eB$ and $\langle Q_{ix} \rangle / c_s$ = 0.011. The latter is quite a bit higher than the peak values shown in Figs. 3, 5, and 7. However, if one uses the time-averaged growth rate of $\gamma_\ell/\Omega_i = 0.0035$ taken from Figs. 1-4 and 6, the quasilinear flux then reduces to $\langle Q_{ix} \rangle / c_s = 0.0041$, which agrees well with the simulation results. Unfortunately, quasilinear diffusion is primarily a linear concept and, as such, there is no apparent reason why it should be related to the steady-state diffusion. In fact, in our three-mode coupling model, χ_i actually vanishes after saturation. One can verify this by using both Eq. (37) and Eq. (39) in the perturbation analysis in calculating χ_i.

The quasilinear electron thermal flux as defined in Eq. (23) is usually small for $|\omega/k_\parallel v_{te}| \ll 1$, because the contribution for the flux mainly comes from the perpendicular pressure perturbation instead of p_e as defined in Eq. (9). Starting with the original drift kinetic equation in $(x, \mu, v_\parallel, t)$,[11] we obtain

$$\langle Q_{ex} \rangle = \sqrt{\pi/2} \, (2/3) \sum_{\mathbf{k}} k_y |\Phi(k)|^2 (\omega_* - \omega_\ell + \omega_{*Te}/2)/k_\parallel v_{te}. \tag{46}$$

The expression is very similar to $\langle \Gamma_{ex} \rangle$ in Eq. (43). The main difference is the sign of ω_{*Te}. Thus the direction of the flux is always outward. Again, Eqs. (28) and (41) give $\langle Q_{ex} \rangle / c_s = 0.00037$, which is much greater than the results shown in Fig. 5. Thus, the linear wave-particle interaction for the electrons becomes

24

inoperative long before the saturation of the instability.

Evidently, quasilinear analysis correlates quite well with the simulation for the ion thermal flux at saturation. However, it is not adequate for describing the quasilinear particle and electron thermal transport. Most of all, the three-mode coupling model totally fails to predict any flux at all in the steady state. The four-mode coupling model, which accounts for the nonlinearly generated $f_i(0,\pm2)$ and is analytically intractable, would provide better agreement with the simulation in terms of saturation level and nonlinear frequency shift. However, even if one carries out the numerical solutions for the four-mode coupling model, past experience has shown that the issue of steady-state transport still cannot be resolved unless one also includes the background fluctuations in the calculation--a rather formidable task.[26]

Instead of the mode coupling approach, we will now proceed to address the problem in a totally different manner by studying the conservation properties of the governing equations. In doing so, we hope to gain some understanding of the physical processes involved in the steady-state transport. We begin by considering a simple periodic system with $\kappa_n = \kappa_{Te} = 0$, $\kappa_{Ti} \neq 0$ and $(k_\perp \rho_s)^2 \ll 1$. From Eqs. (3), (10), and (14), we have

$$(\partial/\partial t)\langle|\nabla_\perp \phi|^2\rangle/2 = \langle(\partial\phi/\partial x_{\|})(u_i - u_e)\rangle,\tag{47}$$

which is the field energy equation, where $\langle\;\rangle$ denotes spatial average. For the adiabatic electrons with $n_e = \phi$, it becomes

$$(\partial/\partial t)\langle|\nabla_\perp \phi|^2 + \phi^2\rangle/2 = \langle(\partial\phi/\partial x_{\|})u_i\rangle,\tag{48}$$

where $|\nabla_\perp \phi|^2 \ll \phi^2$. Multiplying Eq. (2) by f_i/F_{Mi}, integrating the resulting

25

equation in $v_\parallel$, taking the spatial average, and, finally, making use of Eq. (48), we arrive at

$$(\partial/\partial t)\langle \int (f_i^2/\tau F_{Mi})dv_\parallel + |\nabla_\perp \phi|^2 + \phi^2\rangle + \langle(\partial\phi/\partial x_\parallel)\int (f_i^2/F_{Mi})v_\parallel dv_\parallel\rangle = \kappa_{Ti}\langle Q_{ix}\rangle/\tau. \quad (49)$$

In the derivation, the condition $\langle\Gamma_{ex}\rangle = \langle\Gamma_{ix}\rangle = 0$ has been used. This can be verified by multiplying Eq. (3) by $\partial\phi/\partial y$ and taking its spatial average. Equation (49) is the conservation law for the ion thermal flux in the case of adiabatic electrons, where the second term on the left-hand side comes from the nonlinear velocity space term in Eq. (2). Thus, in the true steady state when $\partial/\partial t = 0$, the ion thermal flux may remain finite even in the absence of ion dissipation because of the nonlinear wave-particle interactions. This important insight can help us to explain the simulation results in Figs. 3 and 5, where $\langle Q_{ix}\rangle/c_s \cong 2\times10^{-4}$ for large $\Omega_i t$.

We now proceed to derive the same conservation law based on the fluid equations. After multiplying Eqs. (15) and (16) by u_i and p_i, respectively, and taking their spatial averages, we combine the sum of the resulting equations with Eq. (48) for the adiabatic electrons to obtain

$$(\partial/\partial t)\langle p_i^2/\tau + u_i^2 + |\nabla_\perp \phi|^2 + \phi^2\rangle/2 + = \kappa_{Ti}\langle Q_{ix}\rangle/\tau. \quad (50)$$

Thus, the steady-state ion thermal flux vanishes in a dissipationless system. This is obvious, since the crucial nonlinear velocity space effects, as given by Eq. (49), are now absent in Eq. (50). To understand the influence of electron-ion collisions on the conservation properties in the fluid limit, we can modify Eq. (50) by including Eqs. (10) and (11) to account for the electron responses and by using Eq. (47) for the energy balance. This leads to

$$(\partial/\partial t)\langle p_i^2/\tau + u_i^2 + |\nabla_\perp \phi|^2 + n_e^2\rangle/2 + \nu_{ei}\langle(u_e/v_{te})^2\rangle/2 = \kappa_{Ti}\langle Q_{ix}\rangle/\tau, \tag{51}$$

with the assumption of $\nu_{ei} \gg \omega$ in Eq. (11). Therefore, collisions can indeed enhance $\langle Q_{ix}\rangle$ in the steady state for finite u_e. (A similar equation has been obtained in Ref. 22, which relates $\langle Q_{ix}\rangle$ with ion viscosity.) Although our simulation parameters lie outside the regime of its validity, Eq. (51) still provides us with a trend which is in agreement with the results shown in Fig. 7. A more appropriate conservation law involving Eqs. (1), (2), and (47) can also be constructed, which, in the steady state, gives

$$2\nu_{ei}\langle \int \frac{1}{F_{Mi}} [\partial f_e/\partial(v_\parallel/v_{te}) + (v_\parallel/v_{te})f_e]^2 dv_\parallel\rangle + \langle(\partial\Phi/\partial x_\parallel)\rangle \int (f_i^2/F_{Mi} - f_e^2/F_{Me})v_\parallel dv_\parallel\rangle$$

$$= \kappa_{Ti}\langle Q_{ix}\rangle/\tau, \tag{52}$$

for $|\langle Q_{ix}\rangle| \gg |\langle\Gamma_{ix}\rangle|$. The importance of collisions and velocity space nonlinearities in determining the magnitude of steady-state transport is therefore evident. Since none of these effects are relevant to the nonlinear saturation of the instability, it is not surprising that the relationship is rather tenuous between the quasilinear χ_i given by Eq. (46) and the steady-state χ_i from Eq. (52).

Unfortunately, based on our current understanding, we cannot realistically estimate the steady-state $\langle Q_{ix}\rangle$ due to η_i-modes. However, if the trend observed in the simulation is assumed to be accurate, one can argue that the quasilinear flux can reasonably be construed as an upper bound for the steady-state flux. Thus, from Eqs. (19) and (45), the scaling law for the ion thermal diffusivity can be written as

$$\chi_i \cong (\rho_s/Rq)^{2/3}(\rho_s/\tau L_{Ti})^{1/3}(k_y\rho_s)^{-5/3} cT_e/eB$$

$$\tag{53}$$

$$\propto T_e^{3/2}/B^2L.$$

where $Rq = 1/k_\parallel$ and $L_{Ti} = 1/\kappa_{Ti}$. Likewise, from Eqs. (19) and (41), the scaling for the saturation amplitude can be obtained as

$$\left| e\Phi/T_e \right| \cong (\rho_s/Rq)^{2/3}(\rho_s/\tau L_{Ti})^{1/3}(k_y\rho_s)^{-5/3}. \tag{54}$$

As for the appropriate $k_y\rho_s$ in these equations, one should use the corresponding wave number for the fastest growing mode in the system. A review of various scalings for χ_i, including Eq. (53), has been given by Connor.[23]

As the final topic of this section, let us examine the scaling laws from a different point of view, i.e., using the invariance properties of the fluid ion equations, Eqs. (14)-(16).[23] For simplicity, we have made following assumptions: $\kappa_n = 0$, $(k_\perp\rho_s)^2 << 1$, $n_i = \Phi$ (i.e., adiabatic electrons). [These are the same equations which are the basis for Eq. (50) as well as for the three-mode coupling analysis.] The resulting equations have only two invariant transformations that are consistent with the original ordering of the equations. They are

P1: $t \to t/\alpha$, $x_\perp \to x_\perp$, $x_\parallel \to x_\parallel/\alpha$, $\Phi \to \alpha\Phi$, $u_\parallel \to \alpha u_\parallel$, $p_i \to \alpha p_i$, $\kappa_{Ti} \to \alpha\kappa_{Ti}$, $\chi_i \to \alpha\chi_i$

P2: $t \to \beta t$, $x_\perp \to \beta x_\perp$, $x_\parallel \to \beta x_\parallel$, $\Phi \to \Phi$, $u_\parallel \to \beta u_\parallel$, $p_i \to \beta p_i$, $\kappa_{Ti} \to \beta\kappa_{Ti}$, $\chi_i \to \beta\chi_i$.

The ion thermal diffusivity can be expressed as

$$\chi_i \propto (\kappa_{Ti}\rho_s/\tau)^s (k_\parallel\rho_s)^q (k_\perp\rho_s)^r \rho_s c_s, \tag{55}$$

where $\rho_s c_s = cT_e/eB$. We then have

$$P1: s+q = 1 \quad \text{and} \quad P2: q+r = -1. \tag{56}$$

which give no unique solutions for s, q, and r. However, the solutions of $q = 2/3$, $s = 1/3$, and $r = -5/3$ satisfy Eq. (56) and give the same scaling in Eq. (55) as the mode-coupling result in Eq. (53). If we neglect $\partial\phi/\partial x_\parallel$ in Eq. (15) and $\partial u_i/\partial x_\parallel$ in Eq. (16),[23] the number of allowable transformations increases to three. As such, the coefficients in Eq. (55) can then be uniquely determined and lead again to the results given by Eq. (53). [The fact that the invariance properties studied here are slightly different from those in Ref. 23 is due to the discrepancy in Eq. (14) as mentioned earlier.]

Dropping of the terms, $\partial\phi/\partial x_\parallel$ and $\partial u_i/\partial x_\parallel$, from the governing equations can be justified by noting that they are irrelevant to the linear stability and to the nonlinear saturation for the 3-mode case. However, the ene:gy-like conservation law, Eq. (50), cannot be satisfied without them. Thus, the scaling of Eq. (53) is valid only for the transient period before the steady state sets in. In the steady state, the flux vanishes as predicted by Eq. (50) and the χ_i scaling under the present assumption becomes meaningless. The derivation of a valid scaling law should therefore include kinetic as well as collisional effects. Their influence on the ion thermal flux is underscored by Eq. (52). However, such an attempt, which needs a more complete understanding of the steady-state physics, is beyond the scope of the present paper and will be pursued in due course.

The scaling for the saturation amplitude can be derived by following the same procedure. For the same parameter dependence as χ_i in Eq. (55), the exponents (s, q, r) are again determined by Eq. (56). Thus, a unique scaling identical to the

29

quasilinear result in Eq. (54) can be obtained when we neglect the same two terms in the ion equations. However, unlike the case for χ_i, Eq. (54) can be a valid subset of the general solution given by Eq. (56). This is borne out by the simulation, in which the saturation amplitude stays roughly at the same level in the steady state. Thus, Eq. (54) is not only valid for the quasilinear saturation, it is applicable for the fluctuation amplitude in the steady state as well.

V. SUMMARY AND CONCLUSION

The investigation of the nonlinear behavior of η_i-modes in a simple shearless slab using gyrokinetic particle simulation techniques has provided us with considerable insight into the saturation of the instability and the resulting thermal transport. It is found that the zero-frequency parallel momentum and pressure responses for the ions, generated by the $E \times B$ convection, are responsible for the nonlinear saturation. The saturation amplitude and the quasilinear ion thermal diffusivity are $\left| e\Phi/T_e \right| \cong (\left| \omega_\ell + i\gamma_\ell \right|/\Omega_i)/(k_\perp \rho_s)^2$, and $\chi_i \cong \gamma_\ell/k_\perp^2$, respectively, [see Eqs. (41) and (45)]. These analytical results are in reasonable agreement with the simulation. The corresponding scaling laws are given by Eqs. (53) and (54). However, the simulation results also indicate that there is more than an order of magnitude reduction for the ion thermal diffusivity in the steady state, whereas the amplitude for the fluctuation potential remains roughly constant. On the other hand, if a small amount of electron-ion collisions in the simulation is introduced, a dramatic increase in the steady-state χ_i without any significant change in $\left| e\Phi/T_e \right|$ has been observed. Through the conservation properties of the gyrokinetic equations, we have found that both the collisions and the ion velocity space nonlinearities are related to the steady-state ion thermal flux as indicated by Eq. (52). However, the exact physical process, that contributes

30

to the phase difference between the potential and pressure response and, in turn, gives rise to the steady-state flux, is still unknown. A recent study has shown that particle "bunching" in the configuration space, due to E×B and phase space trapping, is responsible for the electron-drift-wave-induced particle flux.[30] This mechanism may have some bearing on the present η_i-mode problem as well.

An important and rather surprising lesson learned from the prsent work is that even for a seemingly straightforward situation involving a few nearly coherent modes in the simplest conceivable geometry, the nonlinear physics issues associated with the final steady state remain a very difficult problem yet to be completely resolved. This also serve to highlight the rather weak "first priciples" basis for the common use of $\gamma/k_{\perp}^{2}$ scaling and other phenomenological type models for diffusivities in current transport studies. On the computational front, our work here represents a major step forward for simulating an instability with a very low frequency and a very slow growth rate. The new computational techniques have also enabled us to probe deeper into the nonlinear behavior of this very important type of microinstability.

ACKNOWLEDGMENTS

REFERENCES

[1] B. B. Kadomtsev and O. P. Pogutse, in *Reviews of Plasma Physics* (Consultants Bureau, New York, 1970), Vol. 5, p. 249.

[2] L. I. Rudakov and R. Z. Sagdeev, Dokl. Akad. Nauk. SSSR **138**, 581 (1961) [Sov. Phys. Dokl. **6**, 415 (1965)].

[3] B. Coppi, M. N. Rosenbluth, and R. Z. Sagdeev, Phys. Fluids **10**, 582 (1967).

[4] S. Ejima et al., Nucl. Fusion **22**, 1627 (1982).

[5] B. Blackwell and ALCATOR Group, in *Plasma Phys. and Cont. Nucl. Fusion Res.* (Proc. 9th Int. Conf. Baltimore, 1982), Vol. 2 (IAEA, Vienna, 1983) p. 27.

[6] R. J. Groebner, W. W. Pfeiffer, F. P. Blau, K. H. Burrell, E. S. Fairbanks, and R. P. Seraydarian, Nucl. Fusion **26**, 543 (1986).

[7] B. Coppi, S Cowley, P. Detragiache, R. Kulsrud, F, Pegoraro, and W. M. Tang, in *Plasma Phys. and Cont. Nucl. Fusion Res.* (Proc. 10th Int. Conf. London, 1984), Vol. 2 (IAEA, Vienna, 1985) p. 93.

[8] R. R. Dominguez and R. E. Waltz, GA Technologies Inc. Rep. GA-18184 (1986), Nucl. Fusion (to be published).

[9] F. Romanelli, W. M. Tang, and R. B. White, Nucl. Fusion **26**, 1515 (1986).

[10] W. M. Tang Nucl. Fusion **26**, 1605 (1986).

[11] W. W. Lee, J. Comput. Phys. (in press).

[12] R. E. Waltz and G. E. Guest, Phys. Rev. Lett. **42**, 651 (1979).

[13] P. C. Liewer, W. Pfeiffer, and R. E. Waltz, Phys. Fluids **26**, 563 (1983).

[14] M. Greenwald and ALCATOR Group, Phys. Rev. Lett. **53**, 352 (1984)

[15] S. M. Kaye, Phys. Fluids **28**, 2327 (1985).

[16] P. N. Guzdar, L. Chen, W. M. Tang, and P. H. Rutherford, Phys. Fluids **26**, 673 (1983).

[17] W. M. Tang, G. Rewoldt, and L. Chen, Phys. Fluids **29**, 3715 (1986).

[18] See, for example, W. Horton, in *Handbook of Plasma Physics* (North-Holland, Amsterdam, 1984), Vol. 2, p. 383.

[19] T. Antonsen, B. Coppi, and R. Englade, Nucl. Fusion **19**, 641 (1979).

[20] W. Horton, R. D. Estes, and D. Biskamp, Plasma Phys. **22**, 663 (1980).

[21] W. Horton, D. I. Choi, and W. M. Tang, Phys. Fluids **24**, 1077 (1981).

[22] G. S. Lee and P. H. Diamond, Phys. Fluids **29**, 3291 (1986).

[23] J. W. Connor, Nucl. Fusion **26**, 193 (1986).

[24] W. W. Lee, W. M. Tang, and H. Okuda, Phys. Fluids **23**, 2007 (1980).

[25] R. E. Waltz, and R. R. Dominguez, Bull. Am. Phys. Soc. **31**, 1522 (1986).

[26] J. F. Federici, W. W. Lee, and W. M. Tang, Phys. Fluids **30**, 425 (1987).

[27] A. Hasegawa and K. Mima, Phys. Fluids **21**, 87 (1978).

[28] A. Hasegawa and M. Wakatani, Phys. Rev. Lett. **50**, 682 (1983).

[29] W. W. Lee, J. A. Krommes, C. Oberman, and R. A. Smith, Phys. Fluids **27**, 2652 (1984).

[30] A. M. Dimits, W. W. Lee and J. A. Krommes, private communication.

FIGURE CAPTIONS

FIG. 1 Time evolution and frequency spectra for $e\Phi(1,\pm1)/T_e$ with $\eta_i = \infty$ and $\eta_e = 0$ based on adiabatic electrons and gyrokinetic ions.

FIG. 2 Time evolution for $e\Phi(1,\pm1)$ with $\eta_i = \eta_e = \infty$ based on drift kinetic electrons and gyrokinetic ions (a bandpass filter has been applied to the data).

FIG. 3 Time evolution for the fluctuating potential and the ion thermal flux with $\eta_i = \eta_e = 4$ based on adiabatic electrons and gyrokinetic ions.

FIG. 4 Time history for $e\Phi(1,\pm1)/T_e$ with $\eta_i = \eta_e = 4$ and $\nu_{ei}/\Omega_i = 0$.

FIG. 5 Time history for the electron and ion thermal fluxes with $\eta_i = \eta_e = 4$ and $\nu_{ei}/\Omega_i = 0$.

FIG. 6 Time history for $e\Phi(1,\pm1)/T_e$ with $\eta_i = \eta_e = 4$ and $\nu_{ei}/\Omega_i = 0.005$.

FIG. 7 Time history for the electron and ion thermal fluxes with $\eta_i = \eta_e = 4$ and $\nu_{ei}/\Omega_i = 0.005$.
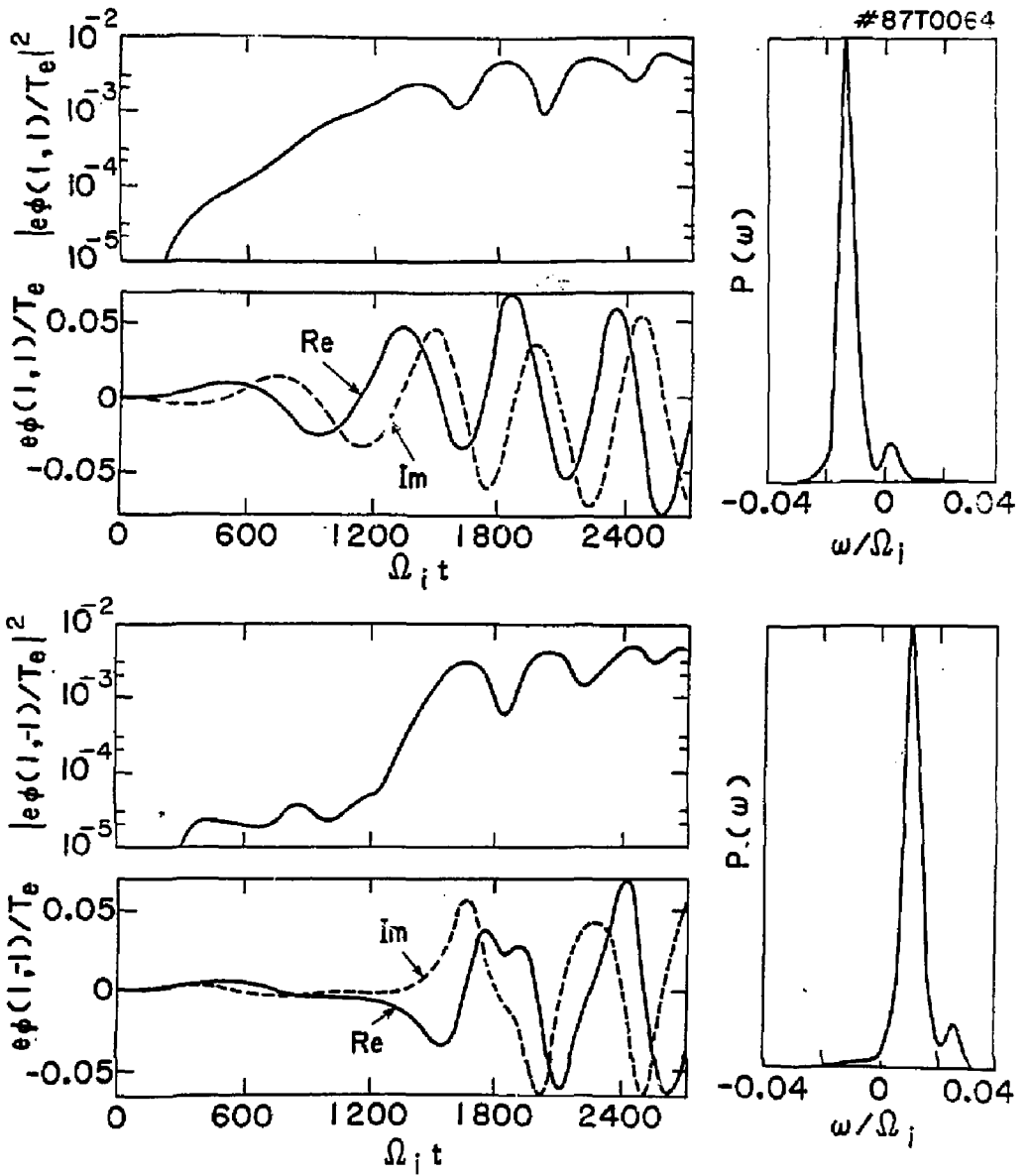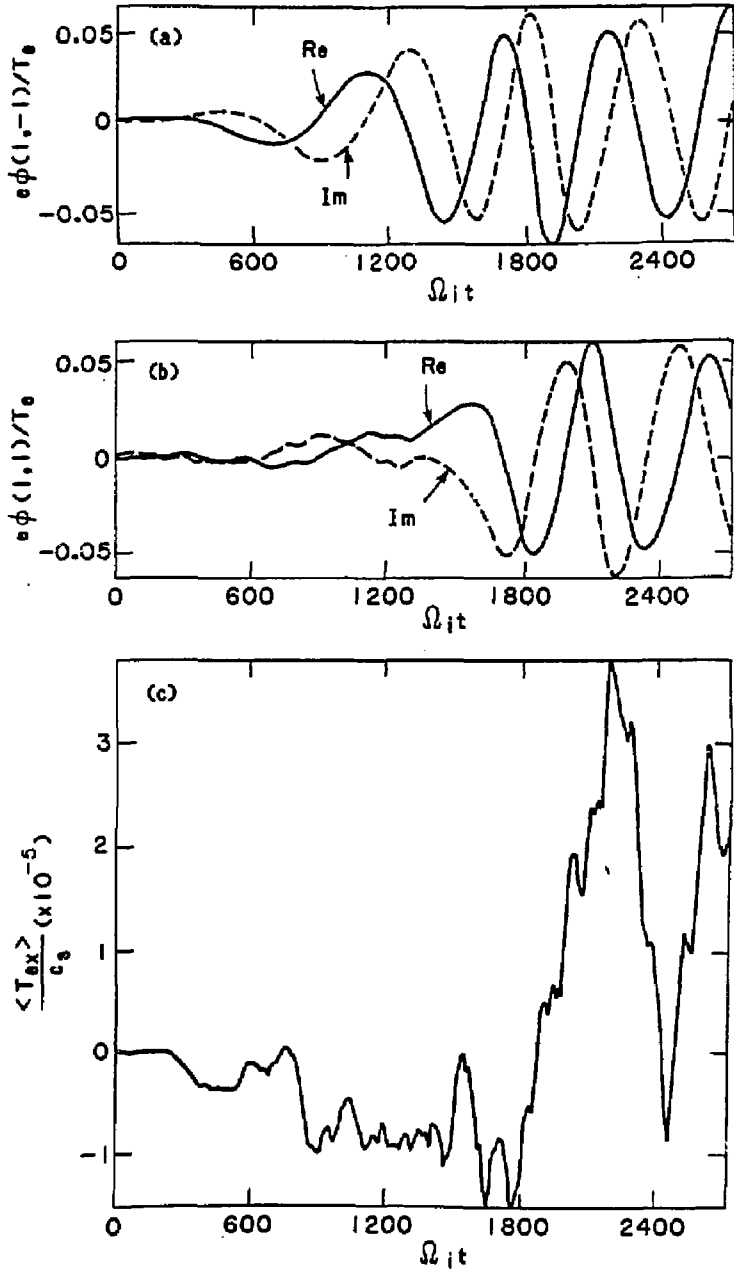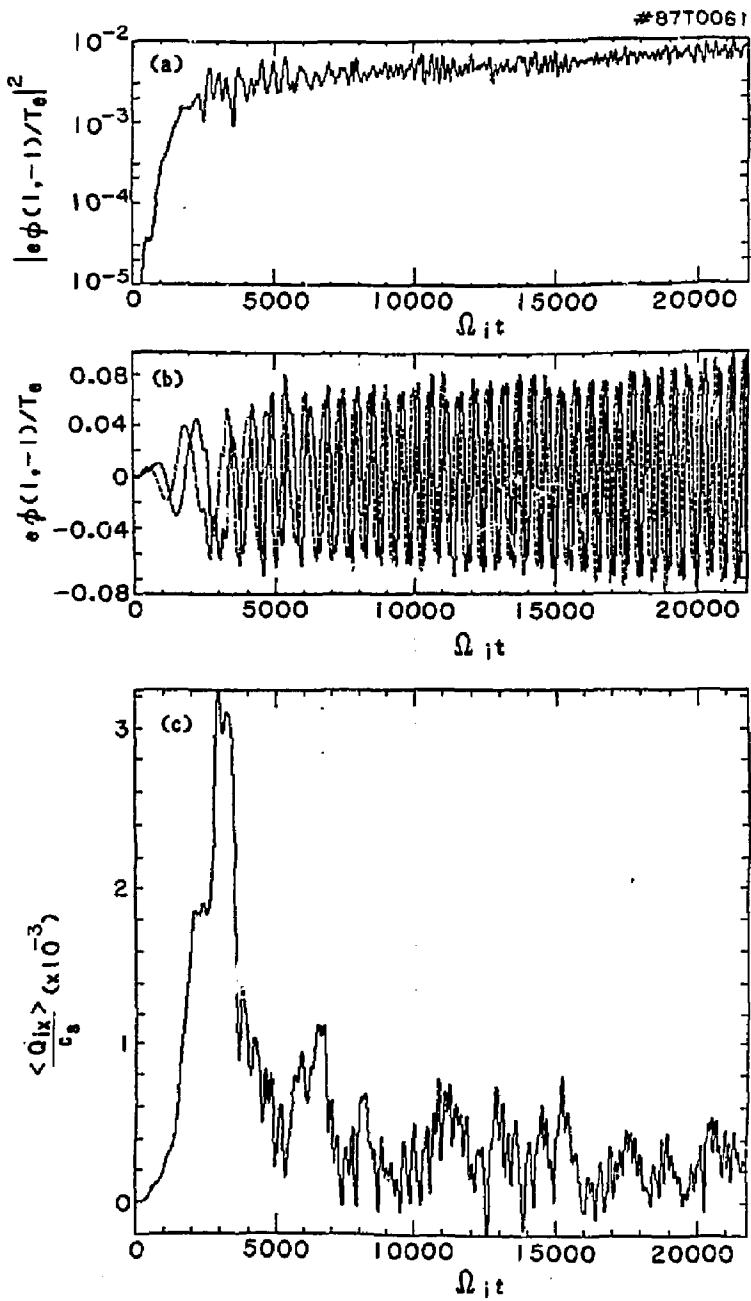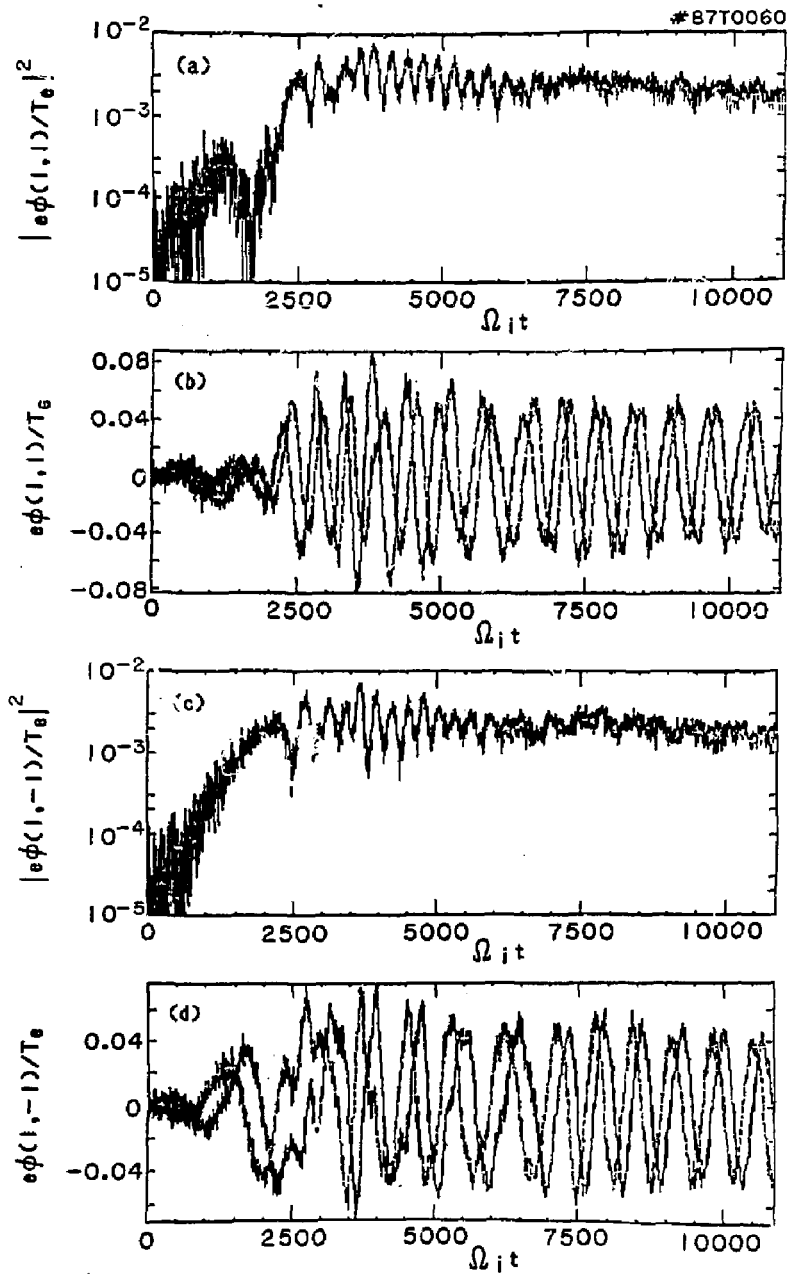
#87T0064

Fig. 1

35

Fig. 2

(a)

$$|e\phi(1,-1)/T_e|^2$$

$\Omega_i t$

(b)

$$e\phi(1,-1)/T_e$$

$\Omega_i t$

(c)

$$\frac{\langle Q_{ix}\rangle}{c_s}\,(\times 10^{-3})$$

$\Omega_i t$

Fig. 3

37

Fig. 4

Fig. 5

Fig. 6

Fig. 7

41
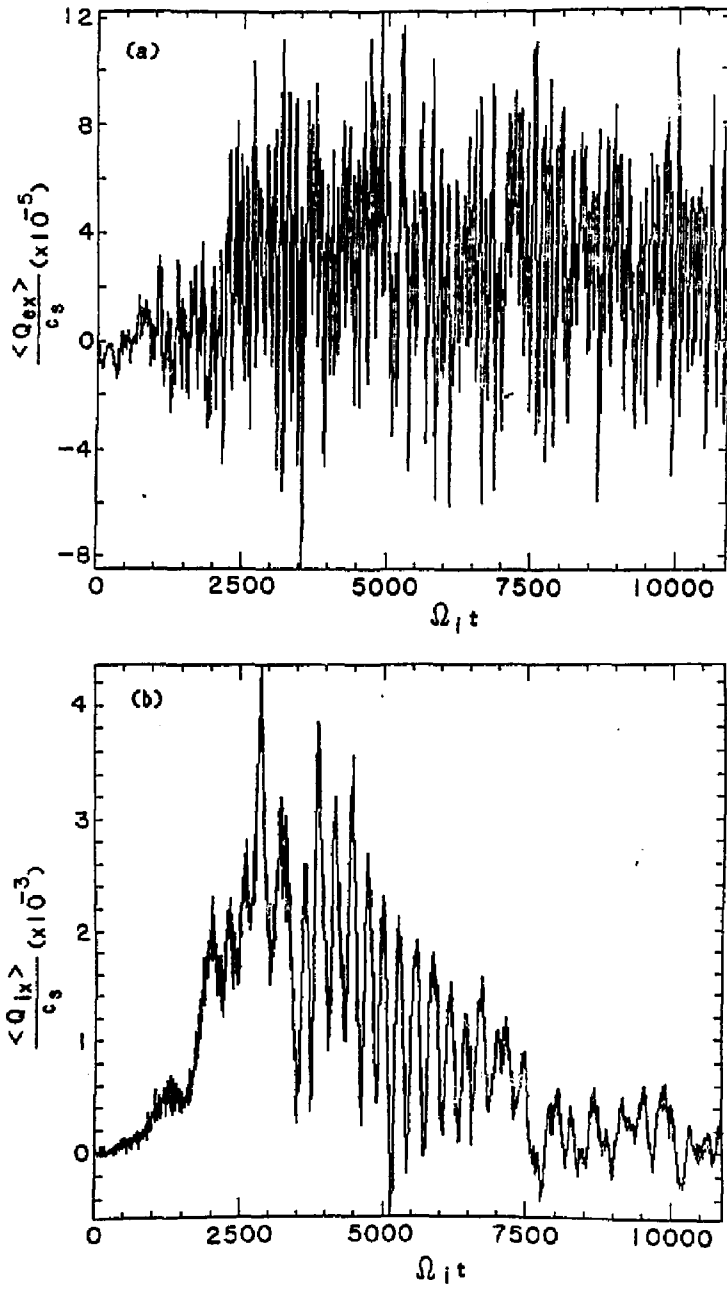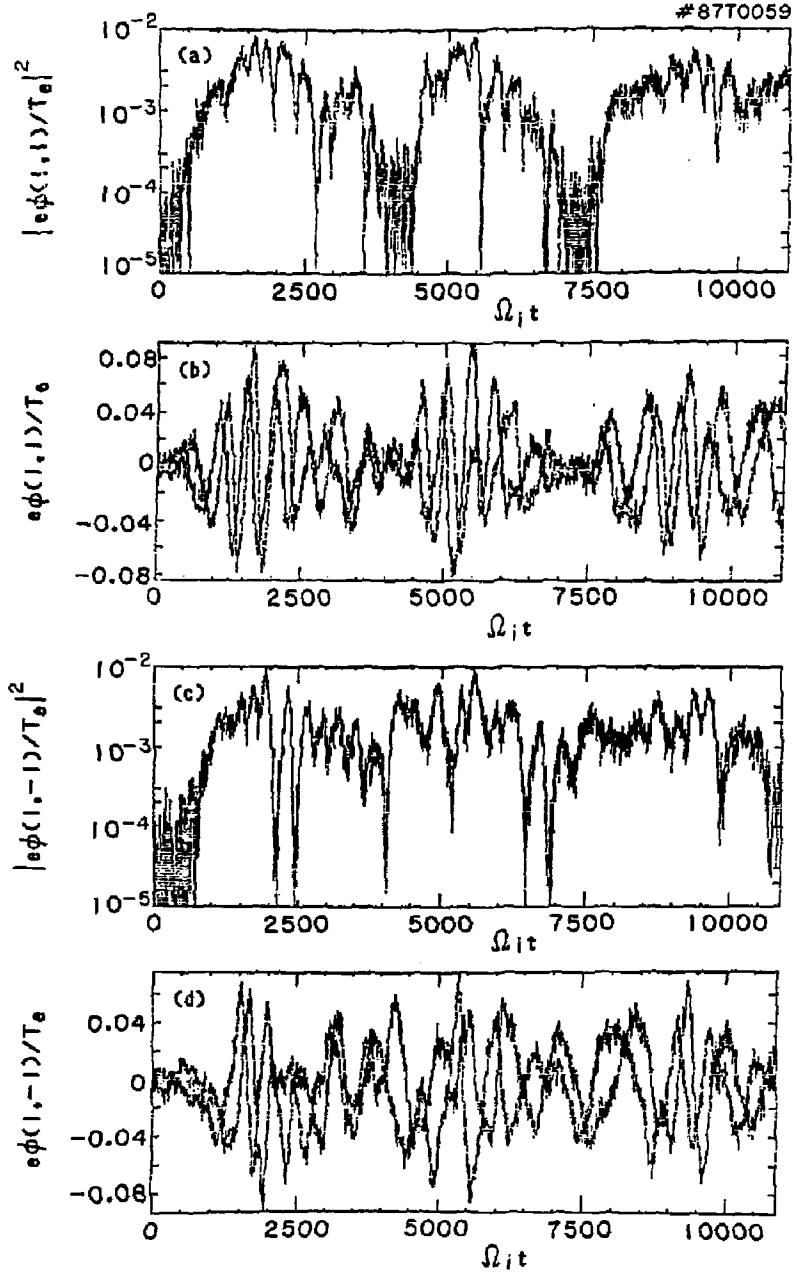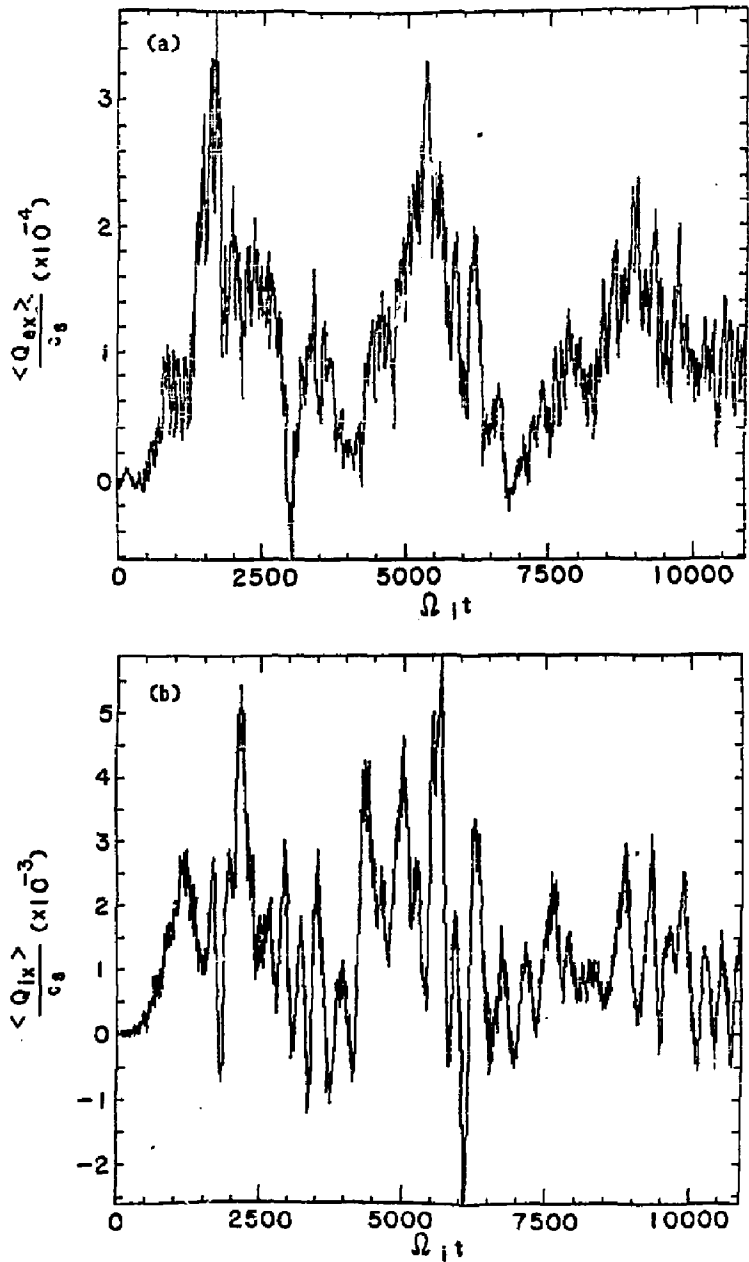
Dr. Frank J. Paoloni, Univ of Wollongong, AUSTRALIA
Prof. M.H. Brennan, Univ Sydney, AUSTRALIA
Plasma Research Lab., Australian Nat. Univ., AUSTRALIA
Prof. I.R. Jones, Flinders Univ., AUSTRALIA
Prof. F. Cap, Inst Theo Phys, AUSTRIA
Prof. M. Heindler,Institut tur Theoretische Physik,AUSTRIA
M. Goossens, Astronomisch Instituut, BELGIUM
Ecole Royale Militaire, Lab de Phys Plasmas, BELGIUM
Com. of European, Dg XII Fusion Prog, BELGIUM
Prof. R. Boucique, Laboratorium voor Natuurkunde, BELGIUM
Dr. P.H. Sakanaka, Univ Estadual, BRAZIL
Instituto De Pesquisas Espaciasi-INPE, BRAZIL
Library, Atomic Energy of Canada Limited, CANADA
Dr. M.P. Bachynski, MPB Technologies, Inc., CANADA
Dr. H.M. Skarsgard, Univ of Saskatchewan, CANADA
Dr. H. Barnard, University of British Columbia, CANADA
Prof. J. Teichmann, Univ. of Montreal, CANADA
Prof. S.R. Sreenivasan, University of Calgary, CANADA
Prof. Tudor W. Johnston, INRS-Energie, CANADA
Dr. C.R. James, Univ. of Alberta, CANADA
Dr. Peter Lukac, Komenskeho Univ, CZECHOSLOVAKIA
The Librarian, Culham Laboratory, ENGLAND
Mrs. S.A. Hutchinson, JET Library, ENGLAND
C. Mouttet, Lab. de Physique des Milieux Ionises, FRANCE
J. Radet, CEN/CADARACHE - Bat 506, FRANCE
Dr. Tom Mual, Academy Bibliographic, HONG KONG
Preprint Library, Cent Res Inst Phys, HUNGARY
Dr. B. Dasgupta, Saha Inst, INDIA
Dr. R.K. Chhajlani, Vikram Univ. INDIA
Dr. P. Kaw, Institute for Plasma Research, INDIA
Dr. Phillip Rosenau, Israel Inst Tech, ISRAEL
Prof. S. Cuperman, Tel Aviv University, ISRAEL
Librarian, Int'l Ctr Theo Phys, ITALY
Prof. G. Rostagni, Univ DI Padova, ITALY
Miss Clelia De Palo, Assoc EURATOM-ENEA, ITALY
Biblioteca, del CNR EURATOM, ITALY
Dr. H. ramato, Toshiba Res & Dev, JAPAN
Prof. I. Kawakami, Atomic Energy Res. Institute, JAPAN
Prof. Kyoji Nishikawa, Univ of Hiroshima, JAPAN
Direc. Dept. Lg. Tokamak Res. JAERI, JAPAN
Prof. Satoshi Itoh, Kyushu University, JAPAN
Research Info Center, Nagoya University, JAPAN
Prof. S. Tanaka, Kyoto University, JAPAN
Library, Kyoto University, JAPAN
Prof. Nobuyuki Inoue, University of Tokyo, JAPAN
S. Mori, JAERI, JAPAN
M.H. Kim, Korea Advanced Energy Research Institute, KOREA
Prof. D.I. Choi, Adv. Inst Sci & Tech, KOREA
Prof. B.S. Liley, University of Walkato, NEW ZEALAND
Institute of Plasma Physics, PEOPLE'S REPUBLIC OF CHINA
Librarian, Institute of Phys., PEOPLE'S REPUBLIC OF CHINA
Library, Tsing Hua University, PEOPLE'S REPUBLIC OF CHINA

Z. LI, Southwest Inst. Physics, PEOPLE'S REPUBLIC OF CHINA
Prof. J.A.C. Cabral, Inst Superior Tecn, PORTUGAL
Dr. Octavian Petrus, AL I CUZA University, ROMANIA
Dr. Johan de Villiers, Plasma Physics, AEC, SO AFRICA
Prof. M.A. Hellberg, University of Natal, SO AFRICA
Fusion Div. Library, JEN, SPAIN
Dr. Lennart Stenfio, University of UMEA, SWEDEN
Library, Royal Inst Tech, SWEDEN
Prof. Hans Wilhelmson, Chalmers Univ Tech, SWEDEN
Centre Phys des Plasmas, Ecole Polytech Fed, SWITZERLAND
Bibliotheek, Fom-Inst Voor Plasma-Fysica, THE NETHERLANDS
Dr. O.D. Ryutov, Siberian Acad Sci, USSR
Dr. G.A. Eliseev, Kurchatov Institute, USSR
Dr. V.A. Glukhikh, Inst Electro-Physical, USSR
Dr. V.T. Tolok, Inst. Phys. Tech. USSR
Dr. L.M. Kovrizhnykh, Institute Gen. Physics, USSR
Prof. T.J.M. Boyd, Univ College N Wales, WALES
Nuclear Res. Establishment, Julich Ltd., W. GERMANY
Bibliothek, Inst. Fur Plasmaforschung, W. GERMANY
Dr. K. Schindler, Ruhr Universitat, W. GERMANY
ASDEX Reading Rm, IPP/Max-Planck-Institut fur
  Plasmaphysik, W. GERMANY
Librarian, Max-Planck Institut, W. GERMANY
Prof. R.K. Janev, Inst Phys, YUGOSLAVIA